ENVIRONMENTAL RESEARCH
LETTERS

Modeling sub-sea permafrost in the East Siberian Arctic Shelf: the Dmitry Laptev Strait

To cite this article: D Nicolsky and N Shakhova 2010 *Environ. Res. Lett.* **5** 015006

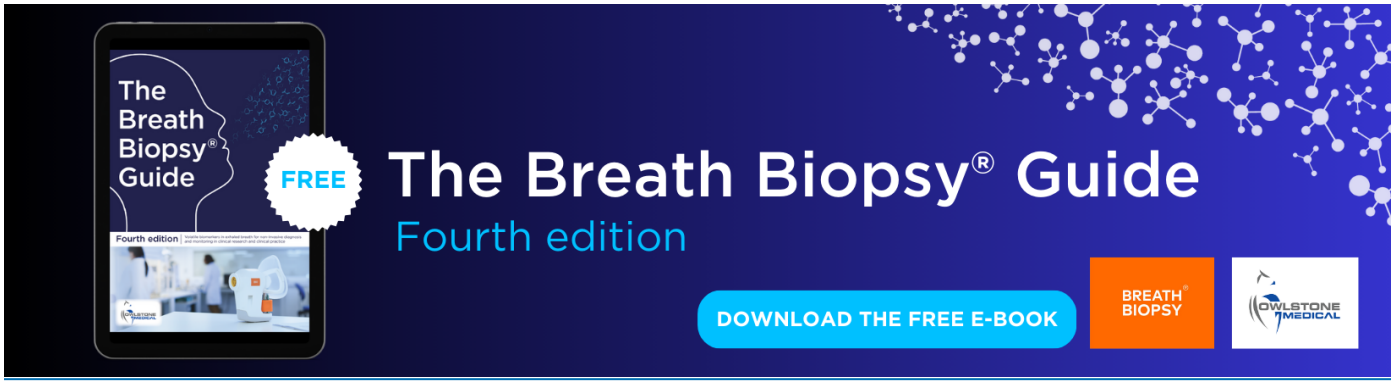

Environ. Res. Lett. **5** (2010) 015006 (9pp) doi:10.1088/1748-9326/5/1/015006

Modeling sub-sea permafrost in the East Siberian Arctic Shelf: the Dmitry Laptev Strait

D Nicolsky[1] **and N Shakhova**[2]

[1] Geophysical Institute, University of Alaska Fairbanks, Fairbanks, AK 99709, USA
[2] International Arctic Research Center, University of Alaska Fairbanks, Fairbanks, AK 99709, USA

E-mail: djnicolsky@alaska.edu and nshakhov@iarc.uaf.edu

Received 8 November 2009
Accepted for publication 17 February 2010
Published 25 March 2010
Online at stacks.iop.org/ERL/5/015006

Abstract
The present state of sub-sea permafrost modeling does not agree with certain observational data on the permafrost state within the East Siberian Arctic Shelf. This suggests a need to consider other mechanisms of permafrost destabilization after the recent ocean transgression. We propose development of open taliks wherever thaw lakes and river paleo-valleys were submerged shelf-wide as a possible mechanism for the degradation of sub-sea permafrost. To test the hypothesis we performed numerical modeling of permafrost dynamics in the Dmitry Laptev Strait area. We achieved sufficient agreement with the observed distribution of thawed and frozen layers to suggest that the proposed mechanism of permafrost destabilization is plausible.

Keywords: sub-sea permafrost, thermokarst, numerical modeling

1. Introduction

Arctic warming can re-introduce carbon, accumulated in terrestrial and sub-sea permafrost for millennia, back into the present day atmosphere and biosphere biogeochemical cycle (ACIA 2004), and consequently might lead to acceleration of certain feedback processes affecting global climate dynamics. The current state of sub-sea permafrost beneath the East Siberian Arctic Shelf (ESAS) is a potential key to understanding whether and how methane, preserved in seabed reservoirs, escapes to the atmosphere. Figure 1 shows the extent of the sub-sea permafrost around the Dmitry Laptev Strait (DLS) and under the Laptev and East Siberian Seas.

Unlike the terrestrial permafrost in the Arctic, which experienced a change in its thermal regime caused by a 6–7 °C mean annual air temperature increase since the last glacial maximum (Frenzel *et al* 1992), sub-sea permafrost has been subjected to additional drastic transformations, e.g. inundation by the ocean, which resulted in warming the permafrost environment by as much as 17 °C (Soloviev *et al* 1987, Kim *et al* 1999, Romanovskii and Hubberten 2001, Romanovskii *et al* 2005). The present understanding of the current thermal state and stability of submarine permafrost in the ESAS, is primarily based on modeling results (Soloviev *et al* 1987, Kim *et al* 1999, Delisle 2000, Romanovskii and Hubberten 2001,

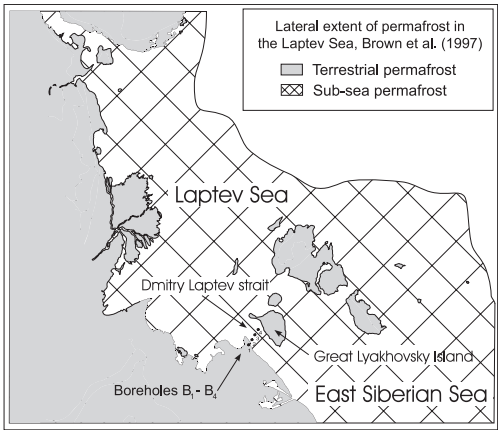

Figure 1. Lateral extent of permafrost in the Laptev and East Siberian Seas, the Dmitry Laptev Strait, and a transect along which several boreholes into sub-sea permafrost were drilled.

Romanovskii *et al* 2005). Two basic mechanisms are proposed to explain permafrost dynamics after the inundation: the so-called upward degradation under geothermal heat flux in the areas underlain by fault zones (Romanovskii and Hubberten 2001), and the so-called downward degradation under the warming effect of large river bodies (Delisle 2000). Modeling results based on either mechanism suggest the existence of open taliks—a body of unfrozen ground connecting sub- and supra-permafrost waters—within limited areas of fault zones and those influenced by large rivers. According to model results in Romanovskii *et al* (2005), the area of seabed endowed with open taliks is less than 5% of the Laptev and East Siberian Seas, and no open taliks can develop within the DLS area due to its distance from large river bodies.

One possible mechanism which allows for formation of open taliks is thawing of the permafrost beneath thaw lakes, submerged several thousand years ago during the ocean transgression, after taliks had already begun to form. Such thaw lakes were abundantly spread on the Laptev Sea coastal plain and their interactions with the ocean are described in Romanovskii *et al* (2000). These authors limit their thermokarst theory to near-shore places, located between the present day shoreline and the isobath −20 m. Noting that the maximum depth in the DLS area does not exceed 15 m, we model permafrost dynamics underneath the submerged thaw lakes, located in the near-shore areas of the ESAS such as in the DLS, by further developing the ideas of Romanovskii *et al* (2000). Outside of the ESAS, in the North American Arctic, research on the sub-sea permafrost was conducted e.g. by Mackay (1972), Osterkamp and Harrison (1985). Several researchers, such as Nixon (1986), Taylor *et al* (1996), attempted modeling of the sub-sea permafrost dynamics on the North American Arctic shelf. One of the key distinctions of their modeling efforts from those of Romanovskii *et al* (2000), Delisle (2000) is that the former included the influence of salt contamination on the permafrost temperature dynamics.

In this work, we try to combine the ideas of Taylor *et al* (1996), Romanovskii *et al* (2000) and show that degradation of the salt-contaminated sub-sea permafrost can lead to formation of open taliks in the DLS area. These taliks can serve as pathways for methane in the marine permafrost, and hence provide a justification for widespread methane observations in the DLS area (Shakhova *et al* 2005, Shakhova and Semiletov 2007).

2. Study area and observations

In a series of ocean transgressions and regressions occurring in the Pleistocene, the DLS area was repeatedly drained and submerged. Under the periodic exposure to the ocean waters, the ground within the DLS became contaminated with ocean salts. In many areas of the ESAS, the salinity of the ground material significantly exceeds that of the ocean (Gigarev 1997). Recall that permafrost describes sediment or rock that has remained below 0 °C for two or more years. Therefore, freezing point depression by saline pore solution can result in unfrozen permafrost (Osterkamp 2001). The DLS area last was last submerged 7000–8000 years ago (Fleming *et al* 1998). Therefore, according to Romanovskii *et al* (2005), no open talik could have yet formed in the strait area from the upward effects of the typical geothermal heat flux. At the same time, the DLS area is distant from large river deltas, and hence this area is not prone to development of taliks due to the downward warming effects of large rivers (Delisle 1998).

In the Late Sartanian, ice complexes were abundantly formed on the drained ESAS. We recall that the ice complexes primarily consist of monolithic ice with inclusions of the ground material. In the DLS area, the ice complexes reached up to 50 m in thickness. Approximately 15 thousand years ago, thermokarst processes started to destroy the ice complexes, both on the shelf and on the coastal lowlands, resulting in thermokarst lakes and depressions forming between 11 and 13 thousand years ago (Romanovskii *et al* 2000). In many areas of the ESAS, the remains of the ice complexes became inundated by the ocean. Note that since the ice complexes primarily consist of fresh ice at the 0 °C phase change temperature, they are not entirely destroyed if the ocean bottom water temperature stays less than 0 °C and chemical erosion is relatively slow.

Presently, remains of the ice complexes are covered by several meters of ocean sediments and are found within the ESAS (Rachold *et al* 2007). According to Overduin *et al* (2007), an approximately 10 m thick ice complex is also found at a depth of 50–60 m below the ground surface of the near-shore zone of the Laptev Sea. It is suggested that this ice complex formed during the Late Sangamon and survives until the present day. This sequence of ocean regressions and transgressions results in the ground material beneath the ESAS ocean bottom having a complicated structure consisting of salt-contaminated sediments, both frozen and thawed, layered with ice complexes (Rachold *et al* 2007, Overduin *et al* 2007).

In the 1980s, an expedition to the DLS took place with the goal of exploring submarine permafrost by drilling several boreholes across the DLS into the ocean bottom (Soloviev *et al* 1987). The observed permafrost temperatures and thicknesses reveal that the upper and lower permafrost boundaries have a strong lateral variation. In figure 2, we show the distribution of frozen and thawed ground across the boreholes, as well as their locations. A layer of frozen ground is observed in each borehole. We emphasize that the ground temperature within the frozen layers of B_2, B_3, and B_4 is between −0.3 and −0.5 °C, implying the frozen layers are not significantly contaminated by salts. In the 133 m deep coastal borehole B_1, one should note that ground material is frozen and its temperature at the 14 m depth is −12.4 °C. Borehole B_3 shows that the upper and lower boundaries of the frozen material are significantly perturbed and also that the thickness of the frozen ground is considerably smaller than those observed in B_2 and B_4. We point out that the regional terrestrial permafrost thickness is believed to be around 400–600 m, however none of the boreholes penetrated the whole layer of permafrost.

3. Modeling assumptions

A difficulty in modeling the present day ground temperature and permafrost distribution lies in specifying a retrospective

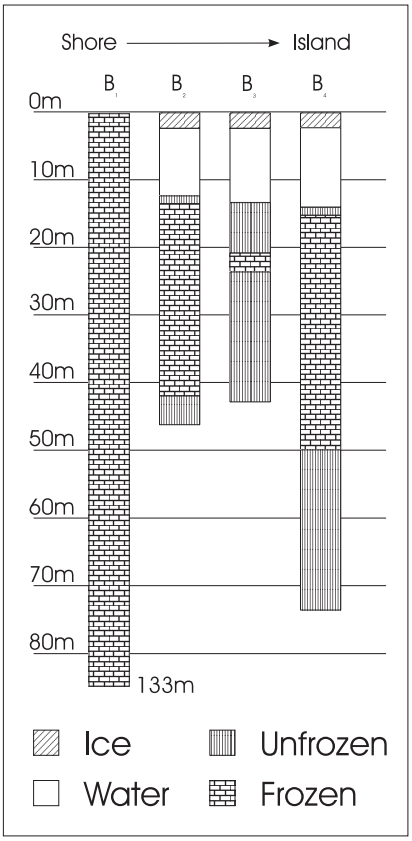

Figure 2. Schematic diagram of layers of frozen and thawed material found in boreholes along the transect (Soloviev *et al* 1987).

climate scenario, including the ground surface temperature dynamics. In Romanovskii and Hubberten (2001), Romanovskii *et al* (2005), it is assumed that ground surface temperature within the study area can be adequately parameterized by the air temperature reconstructed from Vostok ice core data. The eustatic sea level variation can be used to estimate the time at which a certain location became inundated by the Arctic Ocean.

Since there is uncertainty in determining the sea level during the Sangamon Interglacial period, approximately 125 000 years ago, we conservatively approximate that the permafrost thickness in the DLS area was 400–500 m and the temperature profile was determined by geothermal heat flux. According to Soloviev *et al* (1987), the geothermal heat flux within the ESAS typically varies between 40×10^{-3} and 60×10^{-3} W m^{-2} and can reach 100×10^{-3} W m^{-2} in the areas of active faults. Since the DLS is outside the tectonically active zone, and that nearby heat flow measurements show comparable low values (Drachev *et al* 2003), we use the values of 50×10^{-3} and 60×10^{-3} W m^{-2} to simulate the sub-sea permafrost dynamics within the DLS region.

We define the ground temperature, T_g, as the temperature at the bottom of the active layer. The present day mean annual ground temperature, T_p, is $-12\,^{\circ}$C at the coast of the DLS, and so we assume that T_g for the last 125 thousand years is well approximated by

$$T_g = T_v + T_p, \qquad (1)$$

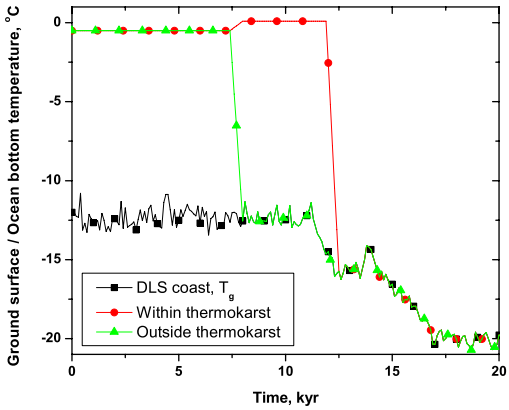

Figure 3. Assumed ground surface/ocean bottom temperature dynamics. The temperature, recovered from the Vostok ice core data and adjusted to model the ground temperature at the DLS coast, T_g, is marked by rectangles. The temperature within and outside the thermokarst depression is marked by circles and triangles, respectively.

where T_v is temperature anomaly (recovered from Vostok ice core data) in relation to T_p (Romanovskii *et al* 2005). Note that thermal insulation of snow, and the thermal offset by the organically enriched mineral soil, is already accounted for in T_p. No trend in precipitation is assumed.

Due to a rapid temperature increase 12 000–13 000 years ago, numerous thermokarst depressions started to develop in the ice complex. In Schwenk *et al* (2006), the seismic image shows depressions in the Laptev Sea bottom topography, a typical thermokarst terrain landscape similar in character to that of the Siberian Lowland. Based on the seismic image, we hypothesize that the thermokarst-affected region is a circle with a 500 m radius. In this work, we model the thermokarst such that the ground surface temperature within this area reached a small positive temperature, e.g. 0.1 °C, over a 1000 year period and remained the same until the area was inundated by the ocean. We note that the assumed temperature at the bottom of the lake is a conservative estimate of water temperature observations (Burn 2002). Figure 3 shows the temperature dynamics within and outside the thermokarst depression.

According to Fleming *et al* (1998), the thermokarst located at 12 m below the present day sea level became inundated approximately 7500 years ago. The present day mean annual water temperature in the DLS is estimated from results of direct year-round measurements to be $-0.5\,^{\circ}$C (Shakhova *et al* 2005). This value is in good agreement with earlier published data on the area (Gigarev 1997). We assume that the ground surface temperature has remained $-0.5\,^{\circ}$C since the inundation. Thawed sediments in the thermokarst pit became contaminated with sea salts and stay thawed at $-0.5\,^{\circ}$C.

4. Numerical modeling

For modeling permafrost dynamics over the timescale of thousands of years, heat conduction is a dominant process, and hence the soil temperature T, (°C) can be simulated by a heat

Table 1. Soil properties of the ground material.

Soil porosity	η	0.2	
Thermal conductivity	λ_f	2.2	(W m^{-1} K^{-1})
Volumetric heat capacity	C_f	1.2×10^6	(J m^{-3} K^{-1})

equation with phase change:

$$L\eta\frac{\partial\theta}{\partial t} + C\frac{\partial T}{\partial t} = \nabla(\lambda\nabla T), \qquad (2)$$

where the quantities $C = C(T, x)$, (J m^{-3} K^{-1}) and $\lambda = \lambda(T, x)$, (W m^{-1} K^{-1}) stand for the volumetric heat capacity and thermal conductivity of soil, respectively; η is the soil porosity; L, (J m^{-3}) is the volumetric latent heat of fusion of water, and θ is the liquid pore water fraction. The thawed and completely frozen ground correspond to $\theta = 1$ and $\theta = 0$, respectively. We note that this equation is applicable when migration of water is negligible, there are no internal sources or sinks of heat, and frost heave is insignificant. We parameterize the thermal properties according to Nicolsky *et al* (2009):

$$C = C_f + \eta(C_w - C_i)\theta, \qquad \lambda = \lambda_f(\lambda_w/\lambda_i)^{\eta\theta}$$

where λ_f and C_f are the thermal properties of completely frozen ground material. The subscripts w and i mark the properties of water and ice, respectively. Values of λ_f and C_f as well as η are listed in table 1.

The quantity $\theta = \theta(T)$ depends on the temperature T, soil texture and salinity. For the coarse grained soils, the quantity θ can be parameterized based on the sodium chloride–water binary phase diagram (Hivon and Sego 1990, 1995) while the temperature T_p can be found by the van't Hoff equation (Lewis and Randall 1961). We discuss the dependence of θ on T for salt-contaminated fine-grained material and its effect on permafrost dynamics later in this letter. The dependence of $\theta(T)$ for two different salt concentrations is shown in figure 4. Note that at any temperature, the ground material with a 35 permille salt concentration has a large liquid pore water fraction $\theta(T)$ compared to that with a 3 permille concentration. The temperatures of the freezing point depression are $-1.8\,^\circ$C and $-0.1\,^\circ$C for the ground material with 35 and 3 permille salt concentrations, respectively. We say that the ground is frozen if its temperature is less than the temperature of the freezing point depression T_p.

In order to reduce the computation time, we model the temperature dynamics in a 2D domain with axial symmetry. In figure 5, we show a 2D computational domain associated with the thermokarst, with the axis of symmetry marked by OO'. The upper boundary is associated with the ground surface near this axis, and with the ocean bottom beyond the approximated 500 m radius. On these boundaries, we specify the ground/ocean bottom temperature within and outside the thermokarst area according to the previously discussed paleoclimatic scenario. On the lower boundary, we specify the constant geothermal heat flux. On the radial boundaries, zero heat flux boundary conditions are prescribed according to the symmetry principle.

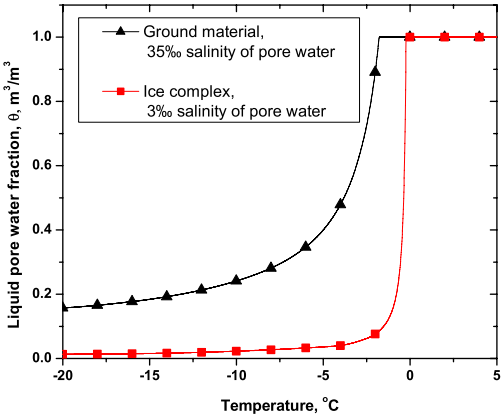

Figure 4. Liquid pore water fraction $\theta(T)$ as a function of temperature T. The curve marked by triangles is associated with salt-contaminated ground material with 35 permille salt concentration, and hence the water content gradually decreases with temperature in 0 °C. The curve marked by rectangles is associated with the ice complex, in which there is a sharp transition between liquid water and ice.

Table 2. Case descriptions.

Case	Salts	Geothermal heat flux (W m^{-2})	Ice complexes (m)
A	No	0.050	0–15
B	Yes	0.050	0–15
C	Yes	0.060	0–15
D	Yes	0.060	0–15, 30–45, 60–75

5. Sensitivity study

In this work, we model several cases of the sub-sea permafrost dynamics within the DLS area. In the first case, we follow the commonly assumed point of view (Romanovskii *et al* 2000, Delisle 2000) and suppose that the ground material is not contaminated by salts. In addition to this assumption, we suppose that an ice complex had formed by the Late Sartanian and that it occupies the upper 15 m of the soil column. The geothermal heat flux is assumed to be 50×10^{-3} W m^{-2}.

The second case is similar to the first. Here, however, the ground material is assumed to be contaminated by the ocean salts, with a 35 permille concentration. The third case is distinguished from the second by assuming that the geothermal heat flux is 60×10^{-3} W m^{-2}. Finally, the fourth case is identical to the third, but with the remains of three ice complexes modeled. In table 2, we summarize the primary differences between each case.

5.1. Case A

In figure 6, we present results of computer modeling in the case of ground material not contaminated by salt. The permafrost distribution and temperatures contours are plotted at several key moments: before development of the thermokarst, after its formation, after inundation by the ocean, and in the present day.

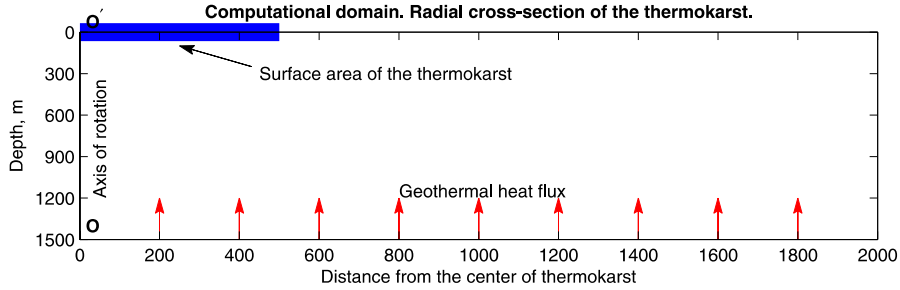

Figure 5. The computational domain with boundary conditions.

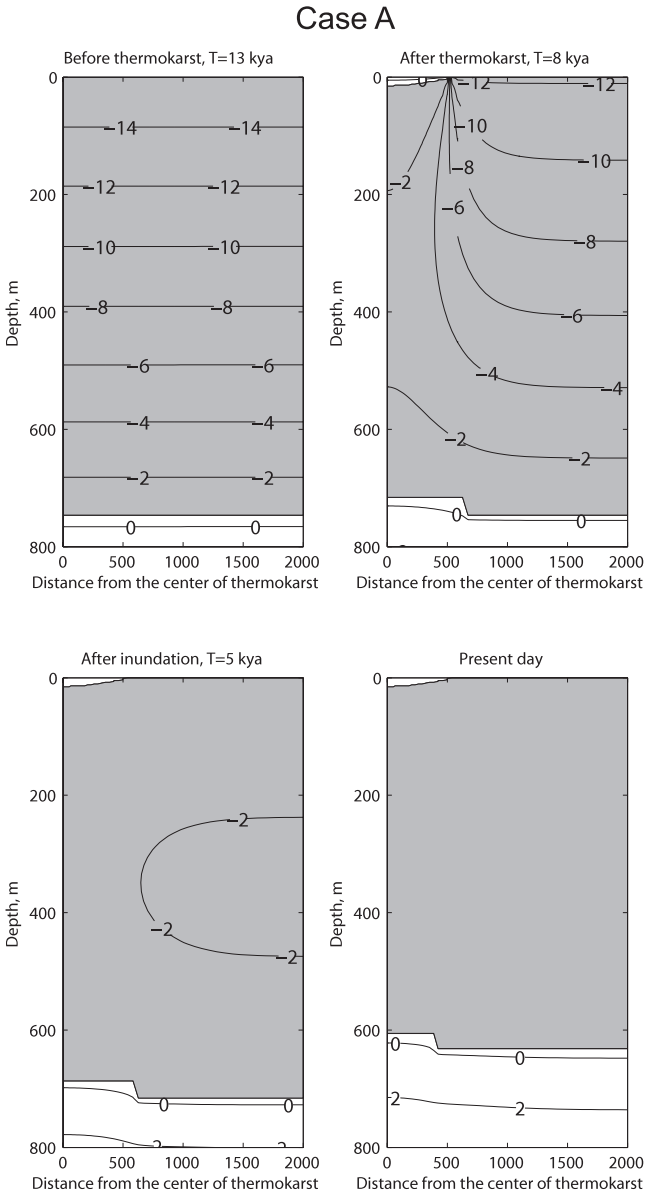

Figure 6. Case A: permafrost and ground temperature 13 000, 8000, 5000 and 0 years ago. The shaded area represents the frozen ground material.

The upper left plot shows the computed temperature at $t = 13\,000$ years ago, before thermokarst depression formation. The shaded area illustrates the frozen ground material. We note that the modeled lower permafrost boundary between 100 and 13 thousand years ago varies between 600 and 800 m. In the upper right plot, we show the temperature at $t = 8000$ years ago, the time 4000 years after initiation of the thermokarst depression and just before inundation. By this time, the lower permafrost boundary is perturbed. However, the simulated permafrost thickness outside the thermokarst area is not significantly decreased from its initial thickness, while the permafrost modeled below the thermokarst depression shows degradation. We emphasize that at $t = 8000$ years ago, the upper permafrost boundary has formed and it reached its maximum depth of approximately 10 m underneath the thermokarst depression. After the inundation, according to our assumptions, the thawed ground within the developed thermokarst becomes contaminated with salts and does not freeze at $-0.5\,^{\circ}$C. The lower left plot shows the computed temperature after the inundation by the ocean $t = 5000$ years ago. The ground temperature in the entire domain is near the temperature of freezing point depression, $T_p \approx -0.1\,^{\circ}$C, and the permafrost slowly degrades from the bottom up. Finally, the lower right plot shows the computed present day temperature profile in the thermokarst and surrounding area. The permafrost thickness outside the thermokarst depression is approximately 600 m, which is in good agreement with other modeling studies that disregard the effects of the sea salts on the permafrost dynamics.

5.2. Case B

In figure 7, we present results of computer modeling for the case of salt-contaminated ground. The permafrost distribution and temperature contours are plotted exactly at the same moments of time as in the above case. We emphasize that the geothermal heat flux in this case is equal to the flux used in the previous case.

In the upper right plot, we show the computed temperature distribution $t = 13\,000$ years ago. The computed temperature profiles corresponding to $t = 13\,000$ years ago in this and the previous case are almost the same. However, due to salt contamination, the freezing point depression temperature T_p is approximately $-2\,^{\circ}$C for the contaminated material. Hence, there is a significant volume of the thawed ground material with temperature less than $0\,^{\circ}$C. Recall that the ground is frozen if its temperature is less that T_p. In all plots, the shaded area represents the frozen ground material.

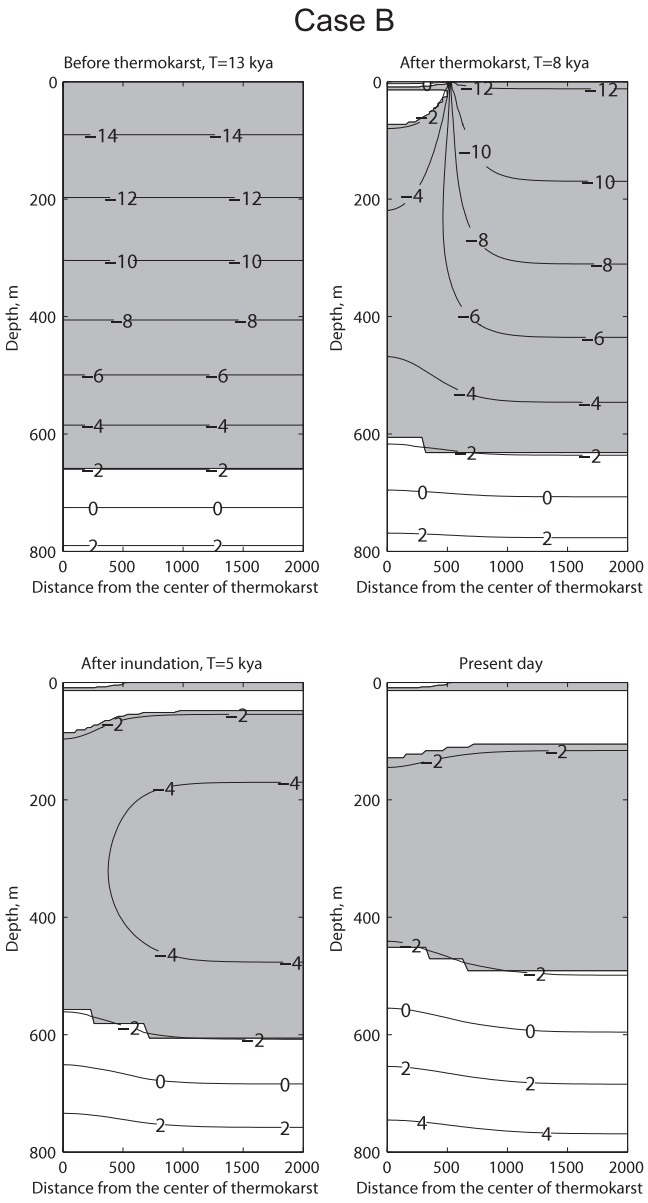

Figure 7. Case B: permafrost and ground temperature 13 000, 8000, 5000 and 0 years ago. The shaded area represents the frozen ground material.

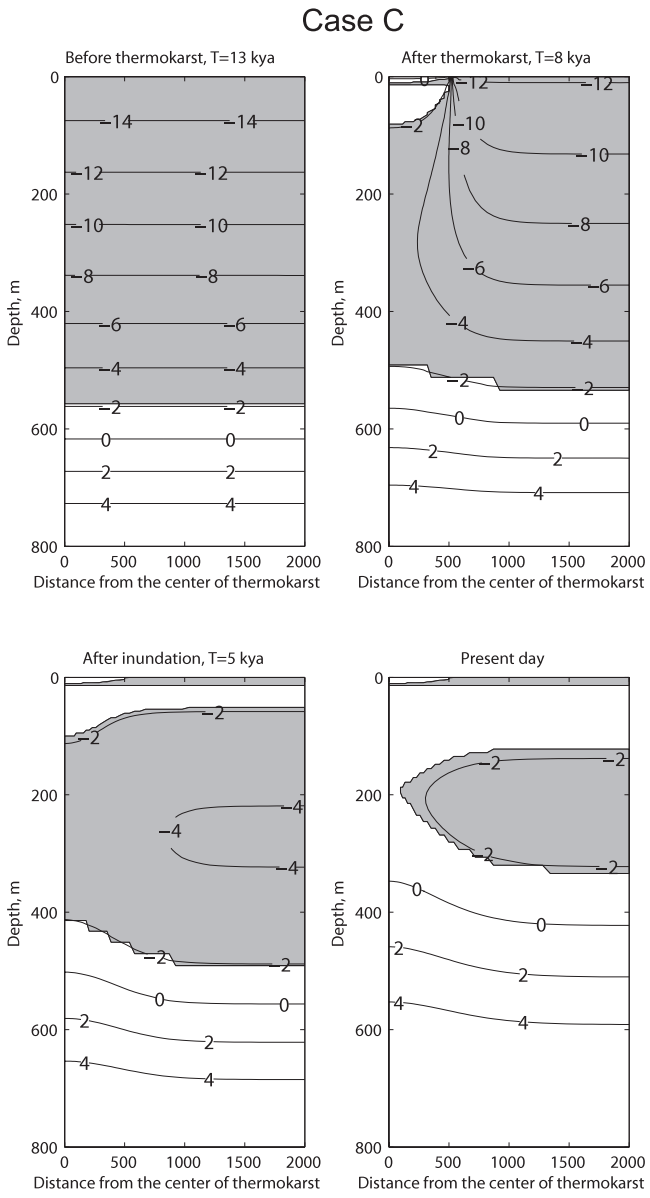

Figure 8. Case C: permafrost and ground temperature 13 000, 8000, 5000 and 0 years ago. The shaded area represents the frozen ground material.

After formation of the thermokarst $t = 8000$ years ago, the computer simulation shows that the ice complex becomes partially degraded with only a thin layer remaining intact. Note that just beneath the ice complex, there is the salt-contaminated ground material having approximately $-2\,^{\circ}\mathrm{C}$, the freezing point depression. During development of the thermokarst, the temperature in the salt-contaminated ground material is less than $0\,^{\circ}\mathrm{C}$, but is higher than $-2\,^{\circ}\mathrm{C}$, and hence the ground material underneath the thermokarst thaws and a talik is formed.

In the lower right figure, we show the simulated distribution of the frozen and thawed ground $t = 5000$ years ago. After inundation by the ocean, the bottom temperature is $-0.5\,^{\circ}\mathrm{C}$, and the partially destroyed ice complex remains intact ($T_{\mathrm{p}} = -0.1\,^{\circ}\mathrm{C}$ for the ice complex), while the salt-contaminated ground beneath the ice complex thaws. Note that boundaries of the frozen salt-contaminated ground material follow the $-2\,^{\circ}\mathrm{C}$ isotherm.

Finally, in the lower right plot, we show the computed distribution of the frozen and thawed material, and the temperature contours. Note that below the ice complex, there is a significant layer of thawed ground material at less than $0\,^{\circ}\mathrm{C}$. The computed results are in qualitative agreement with temperature measurements by Soloviev *et al* (1987), in which a relatively thin layer of frozen material located above the thawed material is observed.

5.3. Case C

In figure 8, we present results of computer modeling in the case of ground material which is also contaminated by salt.

We emphasize that the geothermal heat flux in this case is 60×10^{-3} W m^{-2}, slightly higher than the 50×10^{-3} W m^{-2} flux used in the previous case. Because of the larger value of the geothermal heat flux, the modeled lower permafrost boundary 13 000 years ago is slightly higher than in the previous case. In the upper left plot, we show the temperature contours and the permafrost distribution $t = 13\,000$ years ago.

After formation of the thermokarst, a talik is formed in the salt-contaminated ground material underneath the thermokarst, seen in the upper right plot of figure 8. In the lower left plot, we show the frozen and thawed ground material $t = 5000$ years ago. One of the distinctions between cases B and C is that the lower boundary of the frozen material is more significantly perturbed in case C.

Finally, in the lower right plot, we show results of computer modeling corresponding to the present day. Note that the talik creates a pathway below the thermokarst depression at a depth of approximately 200 m. Through this pathway, methane accumulated beneath the permafrost can potentially escape to the partially destroyed ice complex, and then further to the ocean.

5.4. Case D

In this case, we model dynamics of the case in which three ice complexes are present at different depths. Their locations and thicknesses are listed in table 2. We emphasize that according to our assumptions, these ice complexes are surrounded by salt-contaminated ground.

As in the previous case, during the thermokarst development, a talik is formed in the salt-contaminated ground material, illustrated in the upper right plot of figure 9. The thawed ground material has a temperature less than the ice complexes' temperature of freezing point depression. Therefore, the ice complexes located at depths of 30 and 60 m remain frozen and intact.

After the inundation $t = 5000$ years ago, the computer simulation shows that the talik in the salt-contaminated ground deepens and reaches 100 m. The temperature contours and distribution of the frozen ground after the inundation and at the present day are shown in the lower left and right plots of figure 9, respectively. One of the differences between this case and case C is that the talik underneath the thermokarst is wider in case D. An explanation for the development of the wider talik is that more energy is spent to thaw the salt-contaminated ground and almost none is spent for the phase change transitions within the ice complexes.

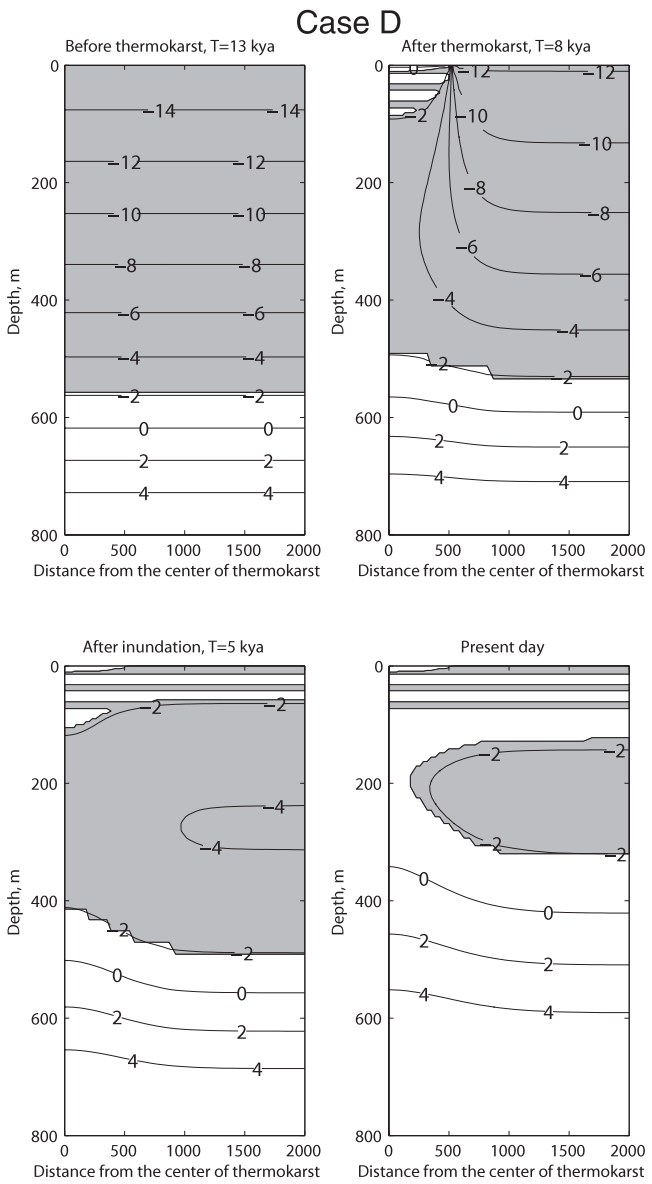

Figure 9. Case D: permafrost and ground temperature 13 000, 8000, 5000 and 0 years ago. The shaded area represents the frozen ground material.

6. Discussion

In this letter, we concentrate on numerical modeling of subsea permafrost observations in the DLS. We emphasize that the goal of this study is to introduce a 2D model of permafrost degradation in salt-contaminated ground underneath inundated thermokarst lakes in the DLS area. An uncertainty in the presented model lies in specifying soil properties such as the thermal parameters C_f and λ_f, the porosity η, and the salt content. The values of λ_f and C_f used in this work are typical for ground materials with small porosity value η. We note that the values of λ_f and C_f are associated with sandy-silty sediments found in the Laptev Sea up to a depth of 400 m (Kim *et al* 1999). The volumetric unfrozen liquid water content θ is typically higher for more finely grained materials (Yershov 1998), and hence qualitatively similar results (more significant thawing) can be expected in cases B, C, and D.

One of the uncertainties in the presented permafrost modeling is related to reconstruction of the ground temperature $T_g = T_v + T_p$, according to (1), in the DLS area. The temperature anomaly T_v recovered from the Vostok ice core data is the global air temperature. In order to simulate the ground temperature T_g in the DLS area, the latitudinal air temperature correction, summer and winter precipitation patterns, and thermal offset due to the organically enriched mineral soil are to be taken into account in order to find the

value of T_p. Note that the latitudinal temperature correction strongly depends on the air mass circulation in the Arctic region. The vegetation and snow cover are strongly influenced by the prevailing temperature and precipitation conditions, and hence depend on the air circulation. Unfortunately, there is small or very limited information regarding the air circulation and precipitation patterns in the DLS area during the last glacial period. This lack of information causes an uncertainty in T_p throughout the previous glacier cycle. The uncertainty in T_p can manifest itself in a significant uncertainty of the present day terrestrial permafrost thickness. However, the temperature regime of the sub-sea permafrost is drastically different from the regime of terrestrial permafrost, since the DLS area was inundated in the Holocene. Since the ocean bottom temperature has not depended on T_p for the last 12 000 years, the uncertainty in T_p during the last glacier cycle leads to a small uncertainty in the present day sub-sea permafrost configuration. For example, an uncertainty in T_p can lead to a thicker or thinner frozen ground layer in cases B, C, and D, but an uncertainty in T_p does not significantly change the geometry of taliks formed underneath inundated thermokarst depressions.

In this work, we used the climate reconstructions by Romanovskii and Hubberten (2001), Romanovskii *et al* (2005). The derived formula (1) for T_g has a bias about 6000 year ago, when the Arctic was warmer than today (CAPE Project Members 2001). The effect of this warmer period on the ocean bottom temperature is still not well understood, but one of the effects of this period is more rapid thawing of salt-contaminated ground material. In the recent study by Burn (2002), the annual mean temperature measurements at the bottom of a lake with similar lateral dimensions ranged between 1.5 and 4.8 °C. Here, we conservatively assume that the mean ground surface temperature within the thermokarst area is 0.1 °C. Preliminary numerical experiments show that if the mean ground surface temperature within the thermokarst area is increased to 1 °C, then the upper ice complex is completely destroyed. Additionally, the presented model does not include chemical erosion and salt redistribution processes within the ground material (Harrison 1982). These processes, can significantly destabilize sub-sea ice complexes and further lead to their destruction. Additionally, we assumed that erosion and sedimentation rates are equal, and that the ocean bottom is stable. Otherwise, further significant destabilization of ice complexes can occur.

We assumed that the modeled permafrost is homogeneous ice-bonded ground material. However, several physical processes, such as anomalies in geothermal heat flux (Romanovskii *et al* 2005), the heating effect of intra-permafrost ground water (Glotov 1994), formation of water pathways due to presence of unfrozen water within frozen ground material (Biggar *et al* 1998), permafrost breaks due to tectonic movement (Cramer and Franke 2005), and sediment settlement and adjustment caused by hydrate decay and manifested as endogenous seismicity (Osterkamp and Harrison 1985) can cause temporal and permanent sub-sea permafrost destabilization. All these processes can contribute to the formation of frozen and thawed ground material layers, and even taliks, in the sub-sea permafrost. However, the action of these aforementioned processes is spatially limited and thus fails to explain seabed permeability and multi-year anomalously high concentrations of methane (Shakhova *et al* 2005).

7. Conclusions

We numerically model sub-sea permafrost dynamics in the DLS since the end of the last glacial period. The simulated permafrost in case A is qualitatively identical to the one modeled by Delisle (2000) and Romanovskii and Hubberten (2001). However, these numerical results contradict the collected observations stating that there is a talik underneath the partially destroyed ice complex (Soloviev *et al* 1987). Numerical results in cases B, C, and D reveal that inclusion of the assumption regarding salt contamination of ground material below the ice complex, drastically affects the computational results and leads to severe thawing of the ground material. According to modeling results, the present day upper boundary of the frozen material outside of the thermokarst depression lies at a depth of 150 m. Unfortunately, the boreholes do not reach this depth, and additional field observations are required to quantitatively verify these modeling efforts.

In cases B, C, and D we observe formation of taliks that are in good qualitative agreement with observations collected in boreholes B_2, B_3, and B_4. In cases C and D the modeled talik at a depth of approximately 200 m creates a pathway that may allow methane, accumulated beneath the permafrost, to escape to the above lying ice complex. We hypothesize that the ice complexes are typically partially, or fully, destroyed by thermal and chemical erosion (Harrison 1982, Yershov 1998), and disturbed by seismic activity (Cramer and Franke 2005). Therefore, they cannot serve as an impermeable obstacle to the methane convection to the ocean bottom and further to the water column. Modeling results in case C and D can be considered as an explanation for the formation of taliks in some areas of the ESAS and as another plausible explanation of the high methane concentration measured in the DLS area.

Acknowledgments

We would like to thank V E Romanovsky, N N Romanovskii, H-W Hubberten, Yu Shur, A Kholodov, S Marchenko, G Delisle, J Stroh, C Burn, and others for all their valuable advice, critique and reassurances along the way. We are thankful to reviewers and the editor for valuable suggestions making the manuscript easier to read and understand. This research was funded by NOAA Cooperative Agreement NA 17RJ1224; NSF OPP ARC 0909546 and 0908788; Russian Foundation for Basic Research, grants 08-05-13572, 08-05-00191-a and 07-05-00050a, and by the State of Alaska. Numerical calculations for this work are supported by a grant of High Performance Computing resources from the Arctic Region Supercomputing Center at the University of Alaska Fairbanks as part of the US Department of Defense HPC Modernization Program.

References

ACIA 2004 *Impacts of a Warming Arctic: Arctic Climate Impact Assessment* (Cambridge: Cambridge University Press) p 139

Biggar K, Haidar S, Nahir M and Jarrett P 1998 Site investigation of fuel spill migration into permafrost *ASCE J. Cold Reg. Eng.* **2** 84–104

Burn C 2002 Tundra lakes and permafrost, Richards Island, western Arctic coast, Canada *Can. J. Earth Sci.* **39** 1281–98

CAPE Project Members 2001 Holocene paleoclimate data from the Arctic: testing models of global climate change *Quat. Sci. Rev.* **20** 1275–87

Cramer B and Franke D 2005 Indications for an active petroleum system in the Laptev Sea, NE Siberia *J. Pet. Geol.* **28** 369–84

Delisle G 1998 Numerical simulation of offshore permafrost development in the Laptev Sea, Siberia *Proc. 7th Int. Conf. on Permafrost (Yellowknife)* ed A Lewkowicz and M Allard, pp 213–9

Delisle G 2000 Temporal variability of sub-sea permafrost and gas hydrate occurrences as function of climate change in the Laptev Sea, Siberia *Polarforchung* **68** 221–5

Drachev S, Kaul N and Beliaev V 2003 Eurasia spreading basin to Laptev Shelf transition: structural pattern and heat flow *Geophys. J. Int.* **152** 688–98

Fleming K, Johnston P, Zwartz D, Yokoyama Y, Lambeck K and Chappell J 1998 Refining the eustatic sea-level curve since the last glacial maximum using far- and intermediate-field sites *Earth Planet. Sci. Lett.* **163** 327–42

Frenzel B, Pécsi M and Velichko A (ed) 1992 *Atlas of Paleoclimates and Paleoenvironments of the Northern Hemisphere: Late Pleistocene-Holocene* (Stuttgart: Gustav Fischer) p 153

Gigarev L 1997 *Oceanic Cryolitozone* (Moscow: Moscow State University) p 320 (in Russian)

Glotov V 1994 Permafrost rocks and ground waters of the Arctic and Pacific Coasts, Nothern Eastern Russia *ICAM-94 Proc.: Permafrost and Engineering Geology* (Magadan: Russian Academy of Sciences Far Eastern Branch) pp 315–9

Harrison W 1982 *Formulation of a Model for Pore Water Convection in Thawing Subsea Permafrost* (*Mitteilungen der Versuchsanstalt für Wasserbau, Hydrologie und Glaziologie*) vol 57 (Zürich: Eidgenössischen Technischen Hochschule)

Hivon E and Sego D 1990 Determination of unfrozen water content in saline permafrost using time-domain-reflectometry (TDR) *5th Canadian Permafrost Conf. (Quebec)* pp 257–62, Nordicana No. 54

Hivon E and Sego D 1995 Strength of frozen saline soils *Can. Geotech. J.* **32** 336–54

Kim B, Grikurov G and Soloviev V 1999 *Land–Ocean System in the Siberian Arctic: Dynamics and History* (Berlin: Springer) pp 683–92 (chapter High Resolution Seismic Studies in the Laptev Sea Shelf: First Results and Future Needs)

Lewis G and Randall M 1961 *Thermodynamics* 2nd edn (New York: McGraw-Hill) revised by K S Pitzer and L Brewer

Mackay J 1972 Offshore permafrost and ground ice, southern Beaufort Sea, Canada *Can. J. Earth Sci.* **9** 1550–61

Nicolsky D, Romanovsky V and Panteleev G G 2009 Estimation of soil thermal properties using *in situ* temperature measurements in the active layer and permafrost *Cold Reg. Sci. Technol.* **55** 120–9

Nixon J 1986 Thermal simulation of subsea permafrost *Can. J. Earth Sci.* **23** 2039–46

Osterkamp T 2001 *Encyclopedia of Ocean Sciences* (New York: Academic) pp 2902–12 (chapter Subsea Permafrost)

Osterkamp T and Harrison W 1985 Sub-sea permafrost: probing, thermal regime, and data analyses, 1975–1981 *Summary Report* (Fairbanks: Geophysical Institute, University of Alaska Fairbanks) p 108

Overduin P, Grigoriev M, Junker R, Rachold V, Kunitsky V, Bolshiyanov D and Schirrmeister L 2007 The expedition COAST I: COAST drilling campaign 2005: subsea permafrost studies in the near-shore zone of the Laptev Sea *Berichte zur Polar- und Meeresforschung* **550** 1–40

Rachold V, Bolshiyanov D, Grigoriev M, Hubberten H-W, Junker R, Kunitsky V, Merker F, Overdum P and Schneider W 2007 Near-shore arctic subsea permafrost in transition *Eos* **88** 149–56

Romanovskii N and Hubberten H-W 2001 Results of permafrost modeling of the lowlands and shelf of the Laptev Sea region, Russia *Permafr. Periglac. Process.* **12** 191–202

Romanovskii N, Hubberten H-W, Gavrilov A, Eliseeva A and Tipenko G 2005 Offshore permafrost and gas hydrate stability zone on the shelf of East Siberian Seas *Geo-Mar. Lett.* **25** 167–82

Romanovskii N, Hubberten H-W, Gavrilov A, Tumskoy V, Tipenko G, Grigoriev M and Siegert C 2000 Thermokarst and land–ocean interactions, Laptev Sea region, Russia *Permafr. Periglac. Process.* **11** 137–52

Schwenk T, Spieß V, Rekant P, Gusev E and Kassens H 2006 Structure of late quarternary sediments and submarine permafrost in the Laptev Sea results from a multi-channel seismic survey during expedition transdrift x *6th Arctic Coastal Dynamic Workshop (Arctic Centre, University of Groningen, The Netherlands)*

Shakhova N and Semiletov I 2007 Methane release and coastal environment in the east Siberian Arctic Shelf *J. Mar. Syst.* **66** 227–43

Shakhova N, Semiletov I and Panteleev G 2005 The distribution of methane on the Siberian Arctic shelves: implications for the marine methane cycle *Geophys. Res. Lett.* **32** L09601

Soloviev V, Ginzburg G, Telepnev E and Mikhaluk Y 1987 *Cryothermia and Gas Hydrates in the Arctic Ocean* (Leningrad: Sevmorgeologia) p 150

Taylor A, Dallimore S and Outcalt S 1996 Late quaternary history of the Mackenzie-Beaufort region, arctic Canada, from modeling of permafrost temperatures. 1. The onshore–offshore transition *Can. J. Earth Sci.* **33** 52–61

Yershov E 1998 *General Geocryology* (Cambridge: Cambridge University Press) p 604